FMRP sustains presynaptic function via control of activity-dependent bulk endocytosis

Katherine Bonnycastle[1,2,3], Peter C. Kind[1,2,3] and Michael A. Cousin[1,2,3*]

1. Centre for Discovery Brain Sciences, Hugh Robson Building, George Square, University of Edinburgh, Edinburgh, Scotland, UK EH8 9XD.
2. Patrick Wild Centre, Hugh Robson Building, George Square, University of Edinburgh, Edinburgh, Scotland, UK EH8 9XD.
3. Simons Initiative for the Developing Brain, Hugh Robson Building, George Square, University of Edinburgh, Edinburgh, Scotland, UK EH8 9XD

*To whom correspondence should be addressed:
Prof. Michael A. Cousin
Telephone +44131 6503259
Email – M.Cousin@ed.ac.uk

Major Classification – Biological Sciences
Minor Classification - Neuroscience

Keywords
FMRP, neuron, endocytosis, vesicle, neurotransmitter, fragile X syndrome

ABSTRACT

Synaptic vesicle (SV) recycling is essential for the maintenance of neurotransmission, with a number of neurodevelopmental disorders linked to defects in this process. Fragile X syndrome (FXS) results from a loss of fragile X mental retardation protein (FMRP) encoded by the *FMR1* gene. FMRP is an established translation repressor, however it also has translation-independent presynaptic roles, including regulation of the trafficking and function of specific ion channels. Since defects in SV recycling are exacerbated during intense neuronal activity, we investigated whether these events were disproportionately affected by the absence of FMRP. We revealed that primary neuronal cultures from a *Fmr1* knockout rat model display a specific defect in activity-dependent bulk endocytosis (ADBE). ADBE is dominant during intense neuronal activity, and this defect resulted in an inability of *Fmr1* knockout neurons to sustain SV recycling during trains of high frequency stimulation. Using a molecular replacement strategy, we revealed that a human FMRP interaction mutant failed to correct ADBE dysfunction in knockout neurons. Therefore, FMRP performs a key role in sustaining neurotransmitter release via selective control of the endocytosis mode, ADBE.

SIGNIFICANCE STATEMENT

Loss of fragile X mental retardation protein (FMRP) results in fragile X syndrome (FXS), however whether its loss has a direct role in neurotransmitter release remains a matter of debate. We demonstrate that neurons lacking FMRP display a specific defect in a mechanism that sustains neurotransmitter release during intense neuronal firing, called activity-dependent bulk endocytosis (ADBE). This discovery provides key insights into mechanisms of brain communication that occur due to loss of FMRP function. Importantly it also reveals ADBE as a potential therapeutic target to correct the circuit hyperexcitabilty observed in FXS.

INTRODUCTION

The communication of information between neurons requires the synchronous fusion of neurotransmitter-containing synaptic vesicles (SVs) during neuronal activity. SVs that are mobilised by action potentials are termed the recycling pool, which can be subdivided into the readily releasable pool (RRP, comprising primed fusion-ready SVs) and the reserve pool (SVs only mobilised during high neuronal activity (1)). Several SV endocytosis modes are sequentially recruited by increasing stimulus intensity to replenish these SV pools (2). Ultrafast endocytosis is dominant during sparse neuronal activity (3), whereas clathrin-mediated endocytosis becomes prevalent during action potential trains (4). Both ultrafast and clathrin-mediated endocytosis saturate during heightened neuronal activity (5, 6), and under these conditions, activity-dependent bulk endocytosis (ADBE) is the dominant endocytosis mode (7). ADBE generates large endosomes directly from the plasma membrane, from which SVs are formed to replenish the reserve pool (8, 9).

The translation repressor fragile X mental retardation protein (FMRP) is located in a number of cellular compartments, including nerve terminals, where it controls the expression of a cohort of presynaptic proteins (10). However, it is also proposed to have protein synthesis-independent functions at the presynapse, such as mediating ion channel gating, activation and density (11). For example, FMRP interacts with Slack potassium channels (12), N-type calcium channels (13) and large conductance voltage and calcium-gated big potassium (BK) channels (14-16). The absence of FMRP at CA3-CA1 hippocampal synapses leads to reduced BK channel activity and excessive action potential broadening (14, 15, 17), resulting in increased presynaptic calcium influx during high frequency stimulation (14, 18). These synapses also display altered short-term plasticity, but only during periods of heightened activity (18, 19). Therefore, presynaptic phenotypes that occur in the absence of FMRP are only revealed during intense neuronal activity (13, 14, 18).

Hyperexcitability of neuronal circuits is a key feature of fragile X syndrome (FXS) (20, 21), one of the most common monogenic causes of intellectual disability (ID) and autism spectrum disorder (22). Most FXS cases are caused by a CGG trinucleotide expansion in the 5' untranslated region of the *FMR1* gene which encodes FMRP, leading to hypermethylation of the promoter and silencing of the *FMR1* gene. Additionally, a point mutation which disrupts polyribosome binding (I304N), is sufficient to cause FXS (23). A different mutation in the *FMR1* gene results in mutant FMRP that is unable to bind and regulate BK channels (R138Q). This mutant has been found in individuals presenting with ID (and in some cases FXS phenotypes, seizures and autism) (24-27). However, it has also been identified in 20 subjects (of which 9 were male) that display no discernable ID (https://gnomad.broadinstitute.org).

Since FMRP appears to be required for optimal presynaptic function specifically during intense neuronal activity, we determined whether SV recycling was disproportionately impacted under these conditions in primary neuronal cultures derived from a recently generated *Fmr1* KO rat model (28). No significant defect in either SV exocytosis or endocytosis was observed, however *Fmr1* KO neurons displayed a robust defect in ADBE. We observed an increase in the SV recycling pool, suggesting homeostatic compensation had occurred. Molecular replacement studies with FMRP mutants in *Fmr1* KO neurons revealed that the ADBE defect was due to loss of BK channel interactions. Therefore, loss of FMRP results in dysfunctional ADBE, which reduces presynaptic performance during periods of intense neuronal activity.

RESULTS

Fmr1 KO hippocampal neurons show no obvious defect in SV recycling

FMRP is proposed to control SV fusion (13), presynaptic action potential duration (18), and short-term synaptic plasticity (18, 19) in different murine models. To determine whether SV exocytosis or

endocytosis were altered in a recently generated *Fmr1* KO rat model (28), we examined SV recycling using synaptophysin-pHluorin (sypHy) in primary hippocampal cultures from KO or wild-type (WT) littermate controls. SypHy consists of the SV protein synaptophysin with a pH-sensitive EGFP (pHluorin) fused to an intraluminal loop (4). Since sypHy reports the pH of its immediate environment, an exocytosis-dependent increase in its fluorescence signal is observed during SV fusion (Figure 1A, B). After endocytosis, sypHy fluorescence is quenched by SV acidification. This loss of fluorescence is an estimate of the kinetics of SV endocytosis, since this is rate-limiting (4, 29). When WT neurons were challenged with a train of 300 action potentials delivered at 10 Hz, they displayed a characteristic sypHy response, with an evoked increase in fluorescence followed by an exponential post-stimulation decrease to baseline. To determine the amount of exocytosis as a proportion of the total SV pool, fluorescence traces were normalised to the sypHy response in the presence of an alkaline solution (to reveal the maximal unquenched signal; Figure 1B). No significant difference in this parameter was observed when WT and KO were compared (WT, 38.2 ± 2.9 % of total SV pool; KO, 40.4 ± 3.7 %, Figure 1C). The time constant, τ, of SV endocytosis was also not significantly different between WT and KO neurons (WT, 34.0 ± 1.4 s; KO 39.3 ± 3.8 s, Figure 1D). Therefore, loss of FMRP does not impair SV exocytosis or endocytosis during low frequency stimulation.

Previous studies examining loss of FMRP function revealed presynaptic defects during high frequency stimulation (13, 17, 18). Therefore, we next examined sypHy responses evoked by a train of 400 action potentials delivered at 40 Hz (Figure 1E-G). Under these stimulation conditions, there was no difference in either the extent of SV exocytosis (WT, 43.3 ± 2.6 % of total SV pool; KO, 39.9 ± 3.9 %, Figure 1F) or the kinetics of SV endocytosis (WT, 31.8 ± 2.9 s; KO, 31.1 ± 2.8 s, Figure 1G). Taken together, this indicates that deletion of *Fmr1* does not play a significant role in SV recycling during either low or high frequency activity.

Fmr1 KO hippocampal neurons have a larger SV recycling pool

If SV pools were increased in our *Fmr1* KO cultures, this may partially explain our observed lack of effect on the extent of SV exocytosis. To determine this, we inhibited SV acidification with the vacuolar-type ATPase inhibitor bafilomycin A1 in sypHy-transfected neurons (30) (Figure 2). This allows SV exocytosis to be visualised without the confound of SV endocytosis. In these experiments, the RRP was mobilised by 40 action potentials (20 Hz), and the remainder of the recycling pool by 1600 action potentials (20 Hz). The resting pool (which cannot be mobilised by action potentials) was revealed by application of an alkaline solution (Figure 2A). We observed no difference in size of the RRP between genotypes (WT, 12.0 ± 0.9 % of total SV pool; KO, 13.6 ± 1.5 %, Figure 2B), however the SV recycling pool was increased in KO cultures (WT, 46.5 ± 2.8 %, KO, 55.2 ± 2.5 % Figure 2C). Thus, the proportions of SVs in different functional pools are shifted in KO cultures, with more SVs in the recycling pool at the expense of those in the resting pool. This adaptation suggests that *Fmr1* KO nerve terminals compensate for reduced functionality by redistributing SVs to pools that are accessible to neuronal activity.

Fmr1 KO hippocampal neurons show a defect in ADBE

The increase in the SV recycling pool observed in *Fmr1* KO neurons could reflect a compensation for a presynaptic defect. Since presynaptic deficiencies in the absence of FMRP are only revealed during high frequency stimulation (13, 17, 18), we next assessed whether a process that is dominant under these conditions, ADBE, was affected in *Fmr1* KO neurons. ADBE was monitored optically using uptake of 40 kDa tetramethylrhodamine (TMR)-dextran, which is a fluid phase marker that is selectively accumulated via this endocytosis mode (7). WT and *Fmr1* KO neurons were challenged with a train of 400 action potentials (40 Hz) to maximally trigger ADBE in the presence of TMR-dextran (7, 31). The number of nerve terminals that perform ADBE are revealed as discrete TMR-dextran fluorescent puncta (Figure 3A, B). There was a significant decrease in TMR-dextran puncta in *Fmr1* KO neurons relative to WT littermate

controls (76.0 ± 5.2 % of WT, Figure 3C). Importantly, this phenotype was not due to synapse loss in the *Fmr1* KO cultures, since there was no difference in nerve terminal numbers as measured by staining for the SV protein SV2A (Supplementary Figure 1). Taken together, these results reveal a small but robust decrease in the number of nerve terminals undergoing ADBE, suggesting that FMRP may be required for this mode of endocytosis.

Fmr1 KO nerve terminals perform less ADBE

TMR-dextran uptake reports the number of nerve terminals undergoing ADBE, not the extent to which ADBE occurs in each nerve terminal (7). Therefore, we applied the fluid phase marker horse radish peroxidase (HRP) during action potential stimulation (40 Hz 10 s) to confirm the ADBE defect in *Fmr1* KO neurons (Figure 3D, E). Quantification of the number of HRP-labelled endosomes revealed a significant reduction in *Fmr1* KO neurons (4.8 ± 0.3 endosomes per nerve terminal) compared to WT (6.2 ± 0.1 endosomes, Figure 3F). The endosome area across both genotypes was not significantly different (Supplementary Figure 2A), nor were the number of HRP-labelled SVs per nerve terminal (Supplementary Figure 2B). This reduction in the generation of bulk endosomes reveals that *Fmr1* KO neurons display a specific defect in both the extent and prevalence of ADBE during intense neuronal activity.

The R138Q FMRP mutant does not correct the ADBE defect in _Fmr1_ KO neurons

To determine the mechanism underlying the control of ADBE by FMRP, we examined the ability of specific loss of function mutants to rescue TMR-dextran uptake in *Fmr1* KO cultures. First, cultures from *Fmr1* KO rats or WT littermate controls were transfected with either an empty fluorescent mCerulean vector (mCer, empty) or mCer plus EGFP-FMRP (FMRP) for 3 days prior to imaging. Overexpression of $FMRP_{WT}$ did not affect evoked TMR-dextran uptake in WT neurons (Figure 4A, B), indicating that excess FMRP has no detrimental effect on ADBE. It also signifies that additional FMRP does not enhance ADBE, as observed with constitutively active Rab11 mutants (32). Importantly, $FMRP_{WT}$ expression was sufficient to fully rescue the impairment in TMR-dextran uptake in *Fmr1* KO neurons (KO empty: 54.1 ± 9.6 % of WT, KO FMRP: 100.0 ± 14.0 %: Figure 4B).

We next exploited the ability of WT FMRP to fully rescue TMR-dextran uptake to perform molecular replacement studies using two loss of function mutants. These were: $FMRP_{I304N}$ - that does not bind ribosomes (33) and $FMRP_{R138Q}$ - that does not bind BK channels (16, 24) (Figure 4C). When these experiments were performed, $FMRP_{WT}$ (100.0 ± 9.8 %) restored TMR-dextran uptake in *Fmr1* KO cultures as previously observed (Figure 4D). TMR-dextran uptake in $FMRP_{I304N}$ expressing neurons was not significantly different to neurons expressing $FMRP_{WT}$ (90.0 ± 8.4 % of $FMRP_{WT}$, Figure 4D). This indicates that FMRP-dependent control of protein translation is dispensable for ADBE. Interestingly, expression of $FMRP_{R138Q}$ failed to restore TMR-dextran uptake in *Fmr1* KO neurons (69.4 ± 5.5 % of $FMRP_{WT}$), with levels equivalent to those observed with an empty vector (67.8 ± 12.1 % of $FMRP_{WT}$, Figure 4D). These results strongly suggest that FMRP controls ADBE through interactions with BK channels.

Defective ADBE in _Fmr1_ KO neurons results in decreased presynaptic performance

Because ADBE is the dominant endocytosis mode during intense neuronal activity (7), the impact of defective ADBE on SV exocytosis may only be revealed during patterns of high frequency stimulation. To determine this, we monitored the amount of sypHy that visited the plasma membrane as a surrogate of neurotransmitter release in response to multiple trains of high frequency stimulation (Figure 5A, B). The prediction was that *Fmr1* KO neurons would not be able to sustain performance to the same extent as WT, due to a lack of new SVs being provided via ADBE (31). Cultures were stimulated with four trains of high frequency action potentials (40 Hz 10 s) separated by 5 min intervals. WT neurons displayed a sequential decrease in the extent of the evoked sypHy response, consistent with a depletion of SVs

available for exocytosis. When the same protocol was performed for *Fmr1* KO neurons, the sypHy response during the final stimulation was significantly lower (38.7 ± 5.7 % of first response) when compared to WT (55.0 ± 4.0 %; Figure 5B). This suggests FMRP sustains neurotransmitter release during increased neuronal activity via its control of ADBE.

DISCUSSION

Loss of FMRP results in dysregulated translation of a specific cohort of mRNAs culminating in altered postsynaptic function (10). However, FMRP also has non-canonical roles at the presynapse, particularly in the control of ion channel trafficking and activity. Disruption of these roles results in presynaptic dysfunction during intense neuronal activity (11, 14, 17). In this study, we reveal that the absence of FMRP translates into a specific defect in ADBE, an endocytosis mode that is dominant during heightened neuronal activity. Furthermore, molecular replacement studies revealed that the R138Q FMRP mutant failed to restore ADBE in *Fmr1* KO neurons. Finally, we demonstrated that presynaptic performance was reduced in *Fmr1* KO neurons during repetitive neuronal activity. This reveals an activity-dependent requirement for FMRP in maintaining neurotransmitter release via the selective control of a SV endocytosis mode.

Previous morphological studies have produced contradictory observations on SV numbers within CA1 nerve terminals in *Fmr1* KO mice *in situ* (18, 19). Here, we provide a functional confirmation that the SV recycling pool is increased in *Fmr1* KO neurons, which may be an adaptation to reduced SV generation due to restricted ADBE. The increased recycling pool in *Fmr1* KO neurons did not result in an increase in the number of SVs fusing during an action potential train during either low or high frequency stimulation, confirming the lack of a direct role for FMRP in SV exocytosis. In contrast, studies in dorsal root ganglion (DRG) neurons suggested that shRNA-induced depletion of FMRP enhanced SV fusion during high frequency stimulation at 37^{o}C (13). Therefore, to confirm a lack of role for FMRP, we also performed experiments at either physiological temperatures or by depleting FMRP with shRNA. In both instances the absence of FMRP had no effect on SV exocytosis (KB, unpublished observations). It is currently unclear why this disparity exists, however in primary cultures of rat hippocampal *Fmr1* KO neurons we can state that there is no obvious SV fusion phenotype.

The R138Q mutation does not affect the role of FMRP in translation regulation (16, 24). Therefore, its ability to rescue defective ADBE in KO neurons supports the hypothesis that presynaptic defects observed in the absence of FMRP are translation-independent (15). The failure of the R138Q to restore ADBE in *Fmr1* KO neurons could be due to the loss of BK channel regulation. BK channels control action potential duration and shape, and, in the absence of FMRP, *Fmr1* KO synapses display enhanced calcium influx due to action potential broadening (14). Although it appears counterintuitive that an endocytosis mode which is triggered by high neuronal activity (36, 37) is inhibited by enhanced calcium influx, ADBE is reduced when stimulus frequency is increased above 40 Hz (7). This suggests that excess cytoplasmic calcium may limit this endocytosis mode. In support, elevated intracellular calcium inhibits various forms of SV endocytosis in both large atypical and small classical central nerve terminals (38-41). A potential mediator of this inhibition may be synaptotagmin-11, the knockdown of which increases ADBE in DRGs (42). Rescue studies identified both C2A and C2B domains of synaptotagmin-11 as essential for this negative regulatory role. However, early biochemical studies indicated that these C2 domains do not bind calcium (43, 44). An intriguing alternative is that the FMRP-dependent control of ADBE does not involve direct modulation of BK channel activity. In this scenario, BK channels act as a docking station to place FMRP in the correct location to facilitate ADBE. Without this interaction FMRP is mislocalized and unable to perform its role. In support, FMRP and its interaction partners, CYFIP2 and NUFIP2 are enriched on bulk endosomes formed via ADBE (32).

An alterative is that the R138Q mutation results in a loss of FMRP function that is independent of BK channels. For example, FMRP binds to methylated arginines and lysines on chromatin via its tandem Tudor (Agenet) domain (45). The R138Q mutation resides within the extreme C-terminus of this domain and this mutant does not support FMRP-dependent roles in the DNA damage response of cells. Furthermore, the FMRP N-terminus interacts with at least 76 different proteins (46), including CYFIP1/2 and NUFIP1/2 (47-49). While the cellular role of most of these proteins are still unclear, CYFIP1/2 are key components of the Wave Regulatory Complex required for actin remodelling (50, 51). Actin dynamics are essential for optimal ADBE (6), suggesting a potentially additional non-canonical action of FMRP. Interestingly, *Cyfip1*$^{+/-}$ neurons display an increased recycling SV pool in primary culture (52), similar to *Fmr1* KO neurons. Therefore, loss of FMRP function in ADBE may be due to disruption of parallel interactions within its N-terminus.

Could this R138Q-dependent defect in ADBE contribute to FXS? A simplistic answer to this question is no, since the R138Q mutation has been identified a cohort of individuals that display no discernable form of ID (https://gnomad.broadinstitute.org). However, there are other explanations. For example, it is possible that the cohort that carry the R138Q mutation display a mild form of ID that was not detected in clinical assessments. Alternatively, other genetic modifiers may compensate for this mutation in these individuals, reducing its impact. Following this logic, this would mean that the R138Q FMRP mutation would have highly variable penetrance, dependent on the genetic composition of each individual subject. Finally, it is plausible that our observed reduction in ADBE reflects a compensatory or homeostatic mechanism to counteract the increased excitability in FXS, which requires BK channel binding for its initiation rather than protein synthesis. Again, this adaptation would not be a homogenous response across the brain, since neurons that display high firing rates would be disproportionately impacted. Therefore, even if reduced ADBE is not a causal mechanism in FXS, it may still be a valuable therapeutic intervention point to correct the circuit hyperexcitabiltity that is observed in both rodent and human models of this disorder (20, 21). Future studies are therefore now required to determine whether modulation of ADBE can sculpt circuit activity in FXS (and other ASD models that display hyperexcitability - such as SynGAP haploinsufficiency disorder (53)). Irrespective of whether ADBE dysfunction contributes to FXS, the role of FMRP in the control of this key event provides valuable new information into the mechanisms of SV recycling that regulate presynaptic function.

In conclusion, we have revealed a specific, activity-dependent defect in ADBE in *Fmr1* KO neurons that provides key insights into both the presynaptic role of FMRP, but also potential to correct the altered circuit function observed in FXS.

MATERIALS AND METHODS

Materials

Unless otherwise specified, all cell culture reagents were obtained from Invitrogen (Paisley, UK). Foetal bovine serum was from Biosera (Nuaille, France). Papain was obtained from Worthington Biochemical (Lakewood, NJ, USA). All other reagents were obtained from Sigma-Aldrich (Poole, UK). Rabbit anti-SV2A was obtained from Abcam (Cambridge, UK; ab32942). Anti-rabbit Alexa Fluor 488 was obtained from Invitrogen (Paisley, UK; A11008). Synaptophysin-pHluorin (sypHy) was provided by Prof. L. Lagnado (University of Sussex, UK). hEGFP-FMRP isoform 1, was obtained from Dr B. Bardoni (INSERM, IPMC CNRS) (54). hEGFP-FMRP$_{R138Q}$ and hEGFP-FMRP$_{I304N}$ were generated using site-targeted mutagenesis (R138Q forward primer GTGCCAGAAGACTTACAGCAAATGTGTGCCAAA; reverse primer TTTGGCACACATTTGCTGTAAGTCTTCTGGCAC: I304N forward primer AAAAATGGAAAGCTGAATCAGGAGATTGTGGAC; reverse GTCCACAATCTCCTGATTCAGCTTTCCATTTTT (mutated bases underlined).

Primary neuronal culture

Animal work was performed in accordance with the UK Animal (Scientific Procedures) Act 1986, under Project and Personal Licence authority and was approved by the Animal Welfare and Ethical Review Body at the University of Edinburgh (Home Office project licence – 7008878). Specifically, all animals were killed by schedule 1 procedures in accordance with UK Home Office Guidelines; adults were killed by exposure to CO_2 followed by decapitation, whereas embryos were killed by decapitation followed by destruction of the brain.

Heterozygous LE-*Fmr1*$^{em1/PWC}$ female rats (28) were mated with WT males to produce either *Fmr1* KO or WT males. Male embryos were taken at e18.5-e19.5 for hippocampal dissection. Hippocampi from each embryo were processed separately to avoid contamination across genotypes. Dissociated primary hippocampal cultures were prepared from embryos as described (55). Briefly, isolated hippocampi were digested in a 10 U/mL papain solution at 37°C for 20 min. The papain was then neutralised using DMEM F12 supplemented with 10 % Foetal bovine serum and 1 % penicillin/streptomycin. Cells were triturated to form a single cell suspension and plated at 5 x 10^4 cells (with the exception of single cell TMR-dextran uptake experiments, 2.5 x 10^4 cells) per coverslip on laminin (10 µg/ mL) and poly-D-lysine coated 25 mm glass coverslips (VWR International Ltd, Lutterworth, UK). Cultures were maintained in Neurobasal media supplemented with 2 % B-27, 0.5 mM L-glutamine and 1% penicillin/streptomycin. After 2-3 days *in vitro* (DIV), 1 µM of cytosine arabinofuranoside (AraC) was added to each well to inhibit glial proliferation.

SypHy imaging

Hippocampal neurons were transfected with sypHy using Lipofectamine 2000 as per manufacturer's instructions between 6-8 DIV and imaged 7 days later as described (55). Transfected neurons were visualised at 500 nm band pass excitation with a 515 nm dichroic filter and a long-pass >520 nm emission filter on a Zeiss Axio Observer D1 inverted epifluorescence microscope (Cambridge, UK). Images were captured using an AxioCam 506 mono camera (Zeiss) with a Zeiss EC Plan Neofluar 40x/1.30 oil immersion objective. Image acquisition was performed using Zen Pro software (Zeiss). Hippocampal cultures were mounted in a Warner Instruments (Hamden, CT, USA) imaging chamber with embedded parallel platinum wires (RC-21BRFS) and challenged with field stimulation using a Digitimer LTD MultiStim system-D330 stimulator (current output 100 mA, current width 1 ms). Imaging time courses were acquired at 4 s intervals while undergoing constant perfusion with imaging buffer (119 mM NaCl, 2.5 mM KCl, 2 mM $CaCl_2$, 2 mM $MgCl_2$, 25 mM HEPES, 30 mM glucose at pH 7.4, supplemented with 10 µM 6-cyano-7-nitroquinoxaline-2,3-dione (CNQX) and 50 µM DL-2-Amino-5-phosphonopentanoic acid (AP-5). NH_4Cl alkaline buffer (50 mM NH_4Cl substituted for 50 mM NaCl) was used to reveal the maximal pHluorin response.

Time traces were analysed using the FIJI distribution of Image J (National Institutes of Health). Images were aligned using the Rigid body model of the StackReg plugin (https://imagej.net/StackReg). Nerve terminal fluorescence was measured using the Time Series Analyser plugin (https://imagej.nih.gov/ij/plugins/time-series.html). Regions of interest (ROIs) 5 pixels in diameter were placed over nerve terminals that responded to the electrical stimulus. A response trace was calculated for each cell by averaging the individual traces from each selected ROI. Fluorescence decay time constants (tau, τ, s) were calculated by fitting a monoexponential decay curve to data from the time point after the end of electrical stimulation.

TMR-dextran uptake

TMR-dextran (ThermoFisher, Loughborough, UK) uptake was performed as described (31). Neurons were mounted on a Zeiss Axio Observer D1 microscope as described above before challenging with 400

action potentials (40 Hz) in the presence of 50 µM of TMR-dextran (40,000 MW) in imaging buffer. The TMR-dextran solution was immediately washed away after stimulation terminated, and images were acquired using 556/25 nm excitation and 630/98 nm emission bandpass filters (Zeiss) while undergoing constant perfusion. Per coverslip of cells, 3-6 different fields of view were imaged. The TMR-dextran puncta in each image were quantified using the Analyze Particles plugin of Image J (NIH, https://imagej.nih.gov/ij/developer/api/ij/plugin/filter/ParticleAnalyzer.html) to select and count particles of 0.23-0.91 μm^2.

Where TMR-dextran uptake was performed on transfected cultures, WT and KO neurons were transfected 3 days prior to imaging with mCerulean plus either WT, I304N or R138Q GFP-FMRP or mCerulean alone. Transfected axons were visualised on *DIV* 13-15 at both 430 nm and 500 nm excitation (long-pass emission filter >520 nm) to ensure co-transfection. Images of transfected neurons and of TMR-dextran were acquired using 470/27 nm and 556/25 nm double band pass filters and emission filters 512/30 nm and 630/98 nm respectively (Zeiss). Per coverslip of cells, 2-8 neurons were imaged. Axon length was calculated using the Simple Neurite Tracer plugin of Image J (NIH, https://imagej.net/SNT). TMR-dextran puncta (0.23-0.91 μm^2) were counted along transfected axons with the final value normalised for axon length. For all experiments, for each condition, at least one unstimulated coverslip was imaged to correct for the background level of TMR-dextran uptake.

Immunofluorescence staining

Immunofluorescence staining was performed as described (31). Briefly, hippocampal neurons were fixed with 4 % paraformaldehyde in PBS for 15 min. Excess paraformaldehyde was quenched with 50 mM NH_4Cl in PBS. Cells were then permeabilized in 1 % bovine serum albumin (BSA) in PBS-Triton 0.1 % solution for 5 min and blocked in 1 % BSA in PBS at room temperature for 1 h. After blocking, cells were incubated in rabbit anti-SV2A (1:200 dilution) for 1 h, after which the cultures were washed with PBS and incubated with fluorescently conjugated secondary antibodies (anti-rabbit Alexa Fluor 488; 1:1000 dilution) for 1 hr. The coverslips were mounted on slides for imaging with FluorSave (Millipore, Darmstadt, Germany).

HRP uptake

Hippocampal cultures were mounted in the RC-21BRFS stimulation chamber and challenged with 400 action potentials (40 Hz) in the presence of 10 mg/ml HRP supplemented imaging buffer. Immediately following the end of stimulation, cultures were washed in imaging buffer to remove non-internalised HRP and fixed with a solution of 4 % paraformaldehyde in 0.1 M Tris buffer. After washing in 0.1 M Tris buffer, HRP was developed with 0.1 % 3,3'-diaminobenzidine and 0.2 % v/v hydrogen peroxide in Tris buffer. After further washing in Tris buffer, cultures were then stained with 1 % osmium tetroxide for 30 min. Samples were then dehydrated using an ethanol series and polypropylene oxide and embedded using Durcupan. Samples were sectioned, mounted on grids and viewed using an FEI Tecnai 12 transmission electron microscope (Oregon, USA). Intracellular structures that were <61 nm in diameter were arbitrarily designated to be SVs, whereas larger structures were considered endosomes. The endosome area was obtained by tracing the circumference using the freehand selections tool in ImageJ and measuring the resulting area. Typically, 30 fields of view were acquired for one coverslip of cells. The average number of HRP-labelled endosomes and SVs per nerve terminal was calculated for each coverslip and represents the experimental n.

Data analysis

Microsoft Excel (Microsoft, Washington, USA) and Prism 6 software (GraphPad software Inc., San Diego USA) were used for data processing and analysis. The experimenter was blinded during both the

acquisition and analysis of data. For all figures, results are presented with error bars as ± SEM, and the n for each condition represents the number of coverslips imaged. For all assays, cells were obtained from at least two cultures, each containing at least three independent preparations from individual embryos.

ACKNOWLEDGEMENTS

This work was supported by grants from the Simons Foundation (529508), The RS McDonald fund and a College of Medicine and Veterinary Medicine studentship. We thank Steven Mitchell for excellent technical assistance.

REFERENCE LIST

1. Alabi AA & Tsien RW (2012) Synaptic vesicle pools and dynamics. *Cold Spring Harb Perspect Biol* 4(8): a013680.

2. Chanaday NL, Cousin MA, Milosevic I, Watanabe S & Morgan JR (2019) The synaptic vesicle cycle revisited: New insights into the modes and mechanisms. *J Neurosci* 39(42): 8209-8216.

3. Watanabe S*, et al* (2013) Ultrafast endocytosis at mouse hippocampal synapses. *Nature* 504(7479): 242-247.

4. Granseth B, Odermatt B, Royle SJ & Lagnado L (2006) Clathrin-mediated endocytosis is the dominant mechanism of vesicle retrieval at hippocampal synapses. *Neuron* 51(6): 773-786.

5. Lopez-Murcia FJ, Royle SJ & Llobet A (2014) Presynaptic clathrin levels are a limiting factor for synaptic transmission. *J Neurosci* 34(25): 8618-8629.

6. Soykan T*, et al* (2017) Synaptic vesicle endocytosis occurs on multiple timescales and is mediated by formin-dependent actin assembly. *Neuron* 93(4): 854-866.e4.

7. Clayton EL, Evans GJ & Cousin MA (2008) Bulk synaptic vesicle endocytosis is rapidly triggered during strong stimulation. *J Neurosci* 28(26): 6627-6632.

8. Cheung G, Jupp OJ & Cousin MA (2010) Activity-dependent bulk endocytosis and clathrin-dependent endocytosis replenish specific synaptic vesicle pools in central nerve terminals. *J Neurosci* 30(24): 8151-8161.

9. Richards DA, Guatimosim C & Betz WJ (2000) Two endocytic recycling routes selectively fill two vesicle pools in frog motor nerve terminals. *Neuron* 27(3): 551-559.

10. Darnell JC & Klann E (2013) The translation of translational control by FMRP: Therapeutic targets for FXS. *Nat Neurosci* 16(11): 1530-1536.

11. Ferron L (2016) Fragile X mental retardation protein controls ion channel expression and activity. *J Physiol* 594(20): 5861-5867.

12. Brown MR*, et al* (2010) Fragile X mental retardation protein controls gating of the sodium-activated potassium channel slack. *Nat Neurosci* 13(7): 819-821.

13. Ferron L, Nieto-Rostro M, Cassidy JS & Dolphin AC (2014) Fragile X mental retardation protein controls synaptic vesicle exocytosis by modulating N-type calcium channel density. *Nat Commun* 5: 3628.

14. Deng PY*, et al* (2013) FMRP regulates neurotransmitter release and synaptic information transmission by modulating action potential duration via BK channels. *Neuron* 77(4): 696-711.

15. Deng PY & Klyachko VA (2016) Genetic upregulation of BK channel activity normalizes multiple synaptic and circuit defects in a mouse model of fragile X syndrome. *J Physiol* 594(1): 83-97.

16. Kshatri A*, et al* (2020) Differential regulation of BK channels by fragile X mental retardation protein. *J Gen Physiol* 152(6): 10.1085/jgp.201912502.

17. Wang XS*, et al* (2014) Activity-dependent regulation of release probability at excitatory hippocampal synapses: A crucial role of fragile X mental retardation protein in neurotransmission. *Eur J Neurosci* 39(10): 1602-1612.

18. Deng PY, Sojka D & Klyachko VA (2011) Abnormal presynaptic short-term plasticity and information processing in a mouse model of fragile X syndrome. *J Neurosci* 31(30): 10971-10982.

19. Klemmer P*, et al* (2011) Proteomics, ultrastructure, and physiology of hippocampal synapses in a fragile X syndrome mouse model reveal presynaptic phenotype. *J Biol Chem* 286(29): 25495-25504.

20. Booker SA*, et al* (2019) Altered dendritic spine function and integration in a mouse model of fragile X syndrome. *Nat Commun* 10(1): 4813.

21. Das Sharma S*, et al* (2020) Cortical neurons derived from human pluripotent stem cells lacking FMRP display altered spontaneous firing patterns. *Mol Autism* 11(1): 52-020-00351-4.

22. Mefford HC, Batshaw ML & Hoffman EP (2012) Genomics, intellectual disability, and autism. *N Engl J Med* 366(8): 733-743.

23. Feng Y*, et al* (1997) FMRP associates with polyribosomes as an mRNP, and the I304N mutation of severe fragile X syndrome abolishes this association. *Mol Cell* 1(1): 109-118.

24. Myrick LK*, et al* (2015) Independent role for presynaptic FMRP revealed by an FMR1 missense mutation associated with intellectual disability and seizures. *Proc Natl Acad Sci U S A* 112(4): 949-956.

25. Sitzmann AF, Hagelstrom RT, Tassone F, Hagerman RJ & Butler MG (2018) Rare FMR1 gene mutations causing fragile X syndrome: A review. *Am J Med Genet A* 176(1): 11-18.

26. Diaz J, Scheiner C & Leon E (2018) Presentation of a recurrent FMR1 missense mutation (R138Q) in an affected female. *Translational Science of Rare Diseases* 3(3-4): 139-144.

27. Collins SC*, et al* (2010) Identification of novel FMR1 variants by massively parallel sequencing in developmentally delayed males. *Am J Med Genet A* 152A(10): 2512-2520.

28. Asiminas A*, et al* (2019) Sustained correction of associative learning deficits after brief, early treatment in a rat model of fragile X syndrome. *Sci Transl Med* 11(494): 10.1126/scitranslmed.aao0498.

29. Atluri PP & Ryan TA (2006) The kinetics of synaptic vesicle reacidification at hippocampal nerve terminals. *J Neurosci* 26(8): 2313-2320.

30. Sankaranarayanan S & Ryan TA (2001) Calcium accelerates endocytosis of vSNAREs at hippocampal synapses. *Nat Neurosci* 4(2): 129-136.

31. Nicholson-Fish JC, Kokotos AC, Gillingwater TH, Smillie KJ & Cousin MA (2015) VAMP4 is an essential cargo molecule for activity-dependent bulk endocytosis. *Neuron* 88(5): 973-984.

32. Kokotos AC, Peltier J, Davenport EC, Trost M & Cousin MA (2018) Activity-dependent bulk endocytosis proteome reveals a key presynaptic role for the monomeric GTPase Rab11. *Proc Natl Acad Sci U S A* 115(43): E10177-E10186.

33. De Boulle K, *et al* (1993) A point mutation in the FMR-1 gene associated with fragile X mental retardation. *Nat Genet* 3(1): 31-35.

34. Clayton EL, *et al* (2010) Dynamin I phosphorylation by GSK3 controls activity-dependent bulk endocytosis of synaptic vesicles. *Nat Neurosci* 13(7): 845-851.

35. Smillie KJ, Pawson J, Perkins EM, Jackson M & Cousin MA (2013) Control of synaptic vesicle endocytosis by an extracellular signalling molecule. *Nat Commun* 4: 2394.

36. Evans GJ & Cousin MA (2007) Activity-dependent control of slow synaptic vesicle endocytosis by cyclin-dependent kinase 5. *J Neurosci* 27(2): 401-411.

37. Wu XS, *et al* (2009) Ca(2+) and calmodulin initiate all forms of endocytosis during depolarization at a nerve terminal. *Nat Neurosci* 12(8): 1003-1010.

38. Cousin MA & Robinson PJ (2000) Ca(2+) influx inhibits dynamin and arrests synaptic vesicle endocytosis at the active zone. *J Neurosci* 20(3): 949-957.

39. Wu XS & Wu LG (2014) The yin and yang of calcium effects on synaptic vesicle endocytosis. *J Neurosci* 34(7): 2652-2659.

40. von Gersdorff H & Matthews G (1994) Inhibition of endocytosis by elevated internal calcium in a synaptic terminal. *Nature* 370(6491): 652-655.

41. Leitz J & Kavalali ET (2016) Ca2+ dependence of synaptic vesicle endocytosis. *Neuroscientist* 22(5): 464-476.

42. Wang C, *et al* (2016) Synaptotagmin-11 inhibits clathrin-mediated and bulk endocytosis. *EMBO Rep* 17(1): 47-63.

43. von Poser C, Ichtchenko K, Shao X, Rizo J & SÃ¼dhof TC (1997) The evolutionary pressure to inactivate. A subclass of synaptotagmins with an amino acid substitution that abolishes Ca2+ binding. *J Biol Chem* 272(22): 14314-14319.

44. Dai H, *et al* (2004) Structural basis for the evolutionary inactivation of Ca2+ binding to synaptotagmin 4. *Nat Struct Mol Biol* 11(9): 844-849.

45. Alpatov R, *et al* (2014) A chromatin-dependent role of the fragile X mental retardation protein FMRP in the DNA damage response. *Cell* 157(4): 869-881.

46. Taha MS, *et al* (2020) Novel FMRP interaction networks linked to cellular stress. *Febs J* Jun 11. doi: 10.1111/febs.15443.

47. Schenck A, Bardoni B, Moro A, Bagni C & Mandel JL (2001) A highly conserved protein family interacting with the fragile X mental retardation protein (FMRP) and displaying selective interactions with FMRP-related proteins FXR1P and FXR2P. *Proc Natl Acad Sci U S A* 98(15): 8844-8849.

48. Bardoni B, Schenck A & Mandel JL (1999) A novel RNA-binding nuclear protein that interacts with the fragile X mental retardation (FMR1) protein. *Hum Mol Genet* 8(13): 2557-2566.

49. Bardoni B*, et al* (2003) NUFIP1 (nuclear FMRP interacting protein 1) is a nucleocytoplasmic shuttling protein associated with active synaptoneurosomes. *Exp Cell Res* 289(1): 95-107.

50. Chen Z*, et al* (2010) Structure and control of the actin regulatory WAVE complex. *Nature* 468(7323): 533-538.

51. Cioni JM*, et al* (2018) Axon-axon interactions regulate topographic optic tract sorting via CYFIP2-dependent WAVE complex function. *Neuron* 97(5): 1078-1093.e6.

52. Hsiao K, Harony-Nicolas H, Buxbaum JD, Bozdagi-Gunal O & Benson DL (2016) Cyfip1 regulates presynaptic activity during development. *J Neurosci* 36(5): 1564-1576.

53. Gamache TR, Araki Y & Huganir RL (2020) Twenty years of SynGAP research: From synapses to cognition. *J Neurosci* 40(8): 1596-1605.

54. Khayachi A*, et al* (2018) Sumoylation regulates FMRP-mediated dendritic spine elimination and maturation. *Nat Commun* 9(1): 757-018-03222-y.

55. Zhang N*, et al* (2015) Phosphorylation of synaptic vesicle protein 2A at Thr84 by casein kinase 1 family kinases controls the specific retrieval of synaptotagmin-1. *J Neurosci* 35(6): 2492-2507.

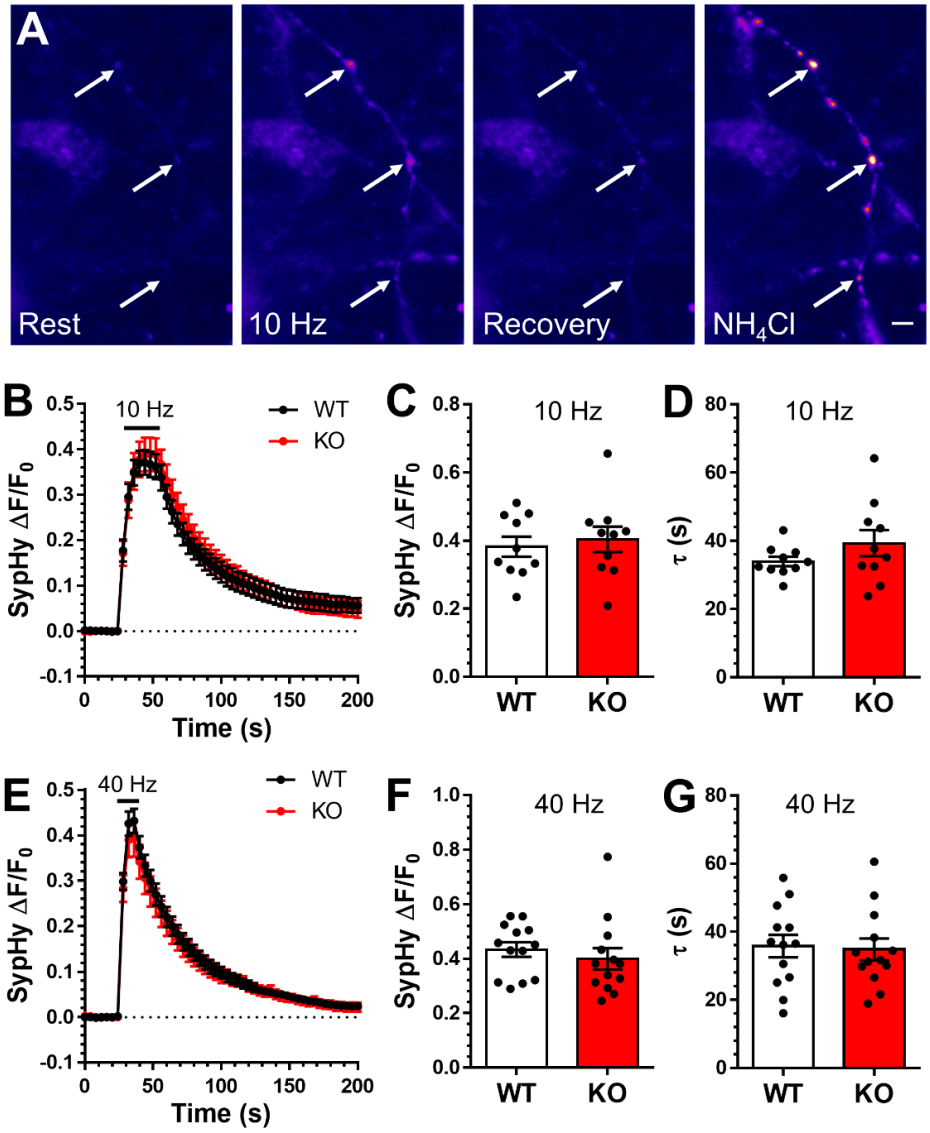

Figure 1. ***Fmr1* KO hippocampal neurons show no obvious defect in SV recycling.** Hippocampal neurons derived from either *Fmr1* KO or WT littermate controls were transfected with sypHy on day *in vitro* (*DIV*) 7 and imaged *DIV* 13-15. Transfected neurons were challenged with a train of action potentials (either 10 Hz 30 s, B-D; or 40 Hz 10 s, E-G) and left to recover for 3 min before exposure to an alkaline buffer (NH_4Cl). A) Representative images of nerve terminals (indicated by arrows) transfected with sypHy at different points during this experiment (Rest, 10 Hz, Recovery and NH_4Cl). Scale bar equivalent to 5 µm. B, E) Mean traces displaying the average sypHy fluorescent response of WT (black) and KO (red) hippocampal neurons in response to 10 Hz (B) or 40 Hz (E) stimulation ± SEM. Traces are $\Delta F/F_0$ and are presented as a fraction of the total SV pool, revealed by NH_4Cl application. Bar indicates the period of stimulation. C, F) Mean sypHy peak heights ± SEM during either 10 Hz (C) or 40 Hz (F) stimulation. D, G) Mean sypHy retrieval time constants (τ ± SEM) following either 10 Hz (D) or 40 Hz (G) stimulation. For 10 Hz experiments n = 10 for both WT and KO. For 40 Hz experiments n = 13 for WT and KO (Unpaired student t test, C, p=0.65; D, p=0.21; F, p=0.48; G, p=0.83).

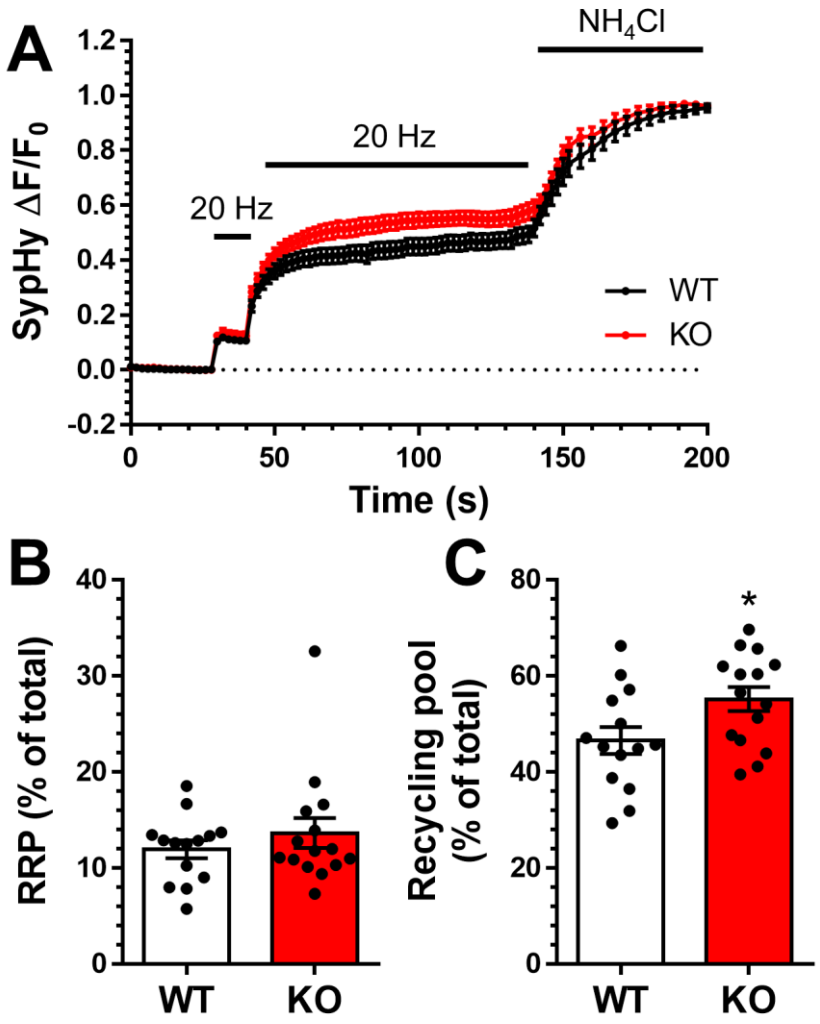

Figure 2. ***Fmr1* KO hippocampal neurons have a larger recycling pool.**
Hippocampal neurons derived from either *Fmr1* KO or WT littermate controls were transfected with sypHy on day *in vitro* (*DIV)* 7 and imaged *DIV* 13-15 in the presence of 1 µM Bafilomycin A1. Transfected neurons were challenged with two trains of action potentials (20 Hz, 2 s and 20 Hz 80 s) before exposure to alkaline buffer (NH_4Cl). A) Mean traces displaying the average sypHy fluorescent response of WT (black) and KO (red) hippocampal neurons is displayed ± SEM. Traces are $\Delta F/F_0$ and normalised to the total SV pool, revealed by NH_4Cl application. Bars indicates the period of stimulation. B) Mean sypHy peak height ± SEM during 20 Hz 2 s stimulation (RRP, % of total pool). C) Mean sypHy peak height ± SEM during 20 Hz 80 s stimulation (Recycling pool, % of total pool). Unpaired Student t-test; B, p=0.37; C, * p = 0.03, n = 14 for WT and n = 15 for KO.

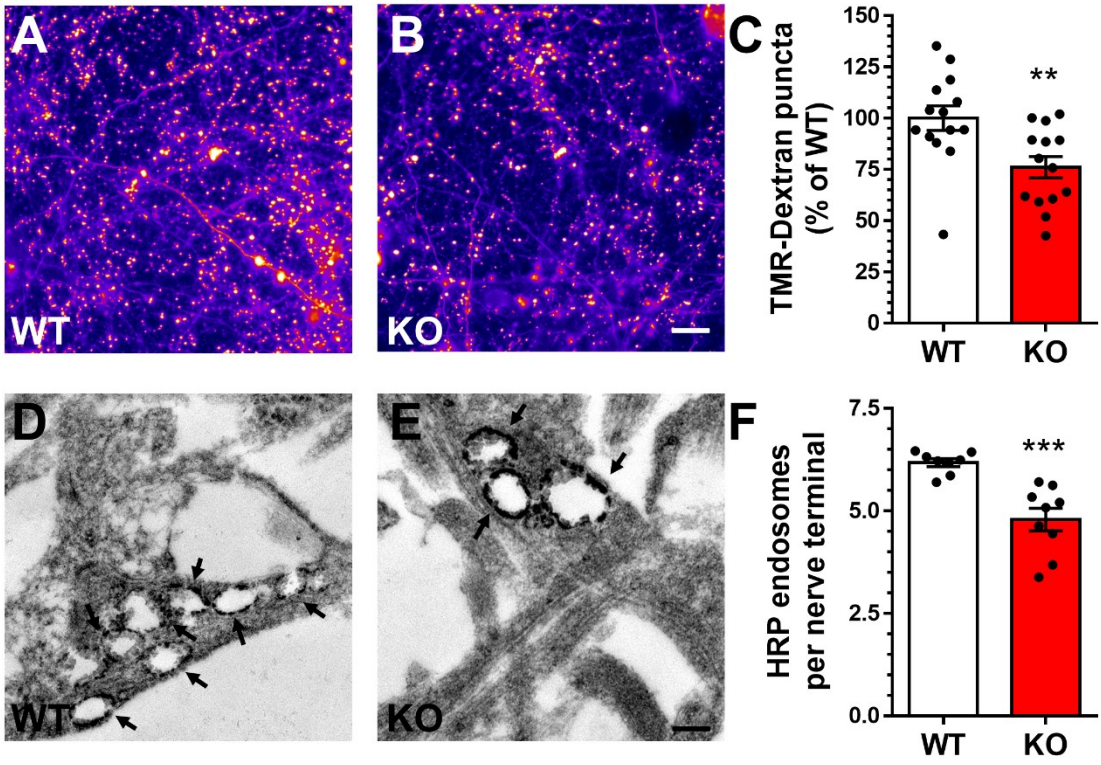

Figure 3. ***Fmr1* KO hippocampal neurons show a defect in ADBE.**
A-C) Hippocampal neurons derived from either *Fmr1* KO or WT littermate controls were challenged with a 40 Hz 10 s action potential train in the presence of 50 μM TMR-dextran at day *in vitro* (*DIV)* 13-15. A, B) Representative images of TMR-dextran-loaded nerve terminals of WT (A) and KO (B) hippocampal neurons. Scale bar represents 30 μm. C) Mean TMR-dextran uptake is presented as a proportion of total WT uptake ± SEM. Unpaired Student t-test ** p = 0.0054; n = 14 for both WT and KO. D-F) Hippocampal neurons derived from either *Fmr1* KO or WT littermate controls were challenged with a 40 Hz 10 s action potential train in the presence of 10 mg/ml HRP at *DIV* 13-15. D, E) Representative images of HRP-labelled endosomes and SVs in WT (D) and KO (E) nerve terminals. Black arrows in indicate HRP endosomes, scale bar represents 200 nm. F) Mean HRP-labelled endosome number per nerve terminal in WT and KO cultures ± SEM. Unpaired Student t-test *** p = 0.0004; n = 8 for WT and n = 9 KO.

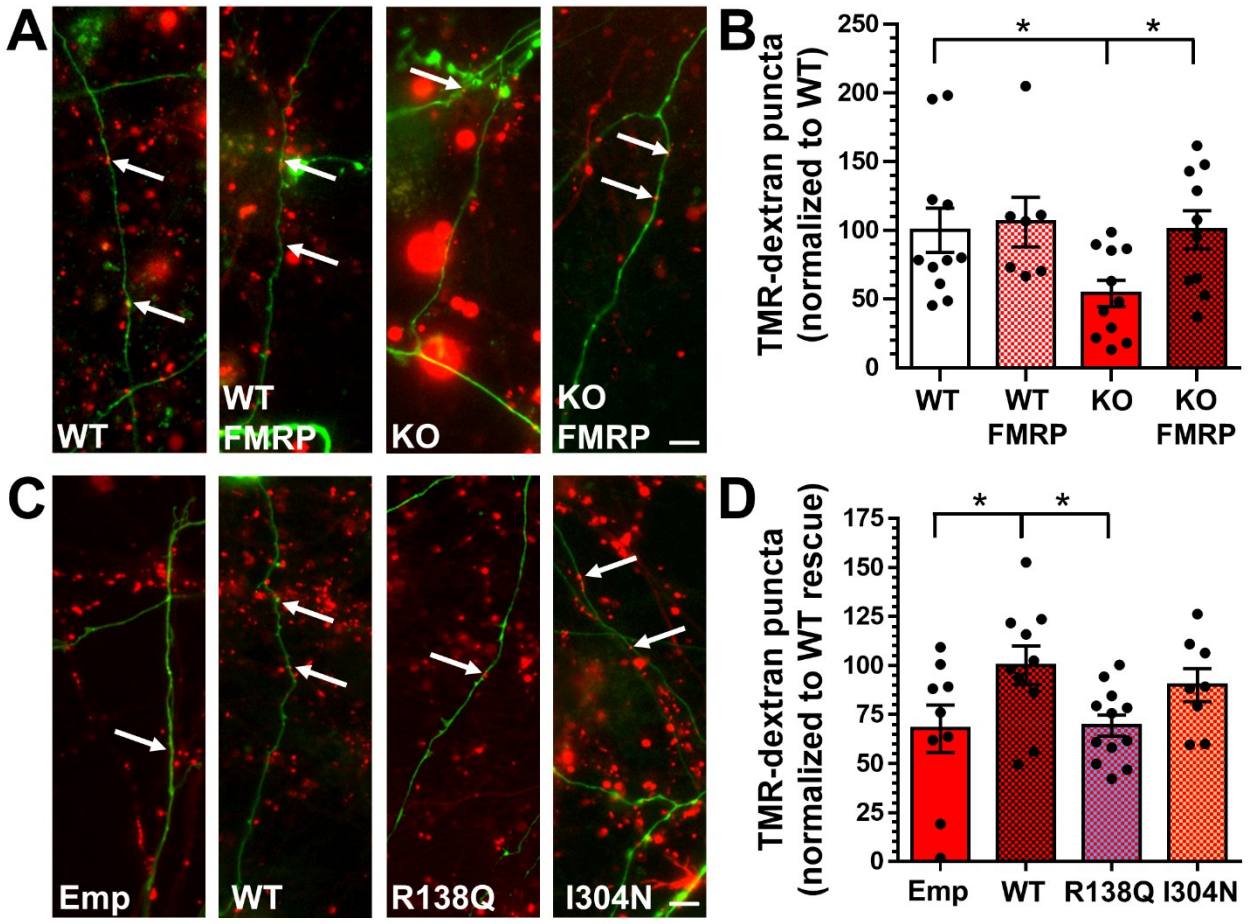

Figure 4. **The R138Q FMRP mutant does not correct the ADBE defect in Fmr1 KO neurons.** A-B) Hippocampal neurons derived from either *Fmr1* KO or WT littermate controls were transfected with mCerulean (empty) or mCerulean and GFP-FMRP (FMRP) 3 days prior to imaging. On day *in vitro* (*DIV)* 13-15, neurons were challenged with a 40 Hz 10 s action potential train in the presence of 50 μM TMR-dextran. A) Representative images of TMR-dextran uptake on axons transfected with empty or FMRP vectors, arrows indicate TMR-dextran puncta. Scale bar represents 10 μm. B) Mean TMR-dextran uptake per 100 μm of transfected axon is presented normalised to WT control ± SEM. 1-way ANOVA with Bonferroni test comparing WT empty and KO empty * p = 0.043; and KO empty and KO FMRP * p=0.048, WT n = 11; WT FMRP n = 7; KO n = 11; KO FMRP n = 10. C-D) Hippocampal neurons derived from *Fmr1* KO embryos were transfected with mCerulean (Emp) or mCerulean and GFP-FMRP (WT), GFP-$FMRP_{R138Q}$ (R138Q), GFP-$FMRP_{I304N}$ (I304N) 3 days prior to imaging. On *DIV* 13-15, neurons were challenged with a 40 Hz 10 s action potential train in the presence of 50 μM TMR-dextran. C) Representative images of TMR-dextran uptake on axons transfected with empty or FMRP vectors, arrows indicate TMR-dextran puncta. Scale bar represents 10 μm. D) Mean TMR-dextran uptake per 100 μm of transfected axon is presented normalised to $FMRP_{WT}$ control ± SEM. 1-way ANOVA with Dunnett's test comparing all values to WT, empty * p= 0.043, R138Q * p= 0.038,Emp n = 8; WT n = 10; R138Q n =12; I304N n = 8.

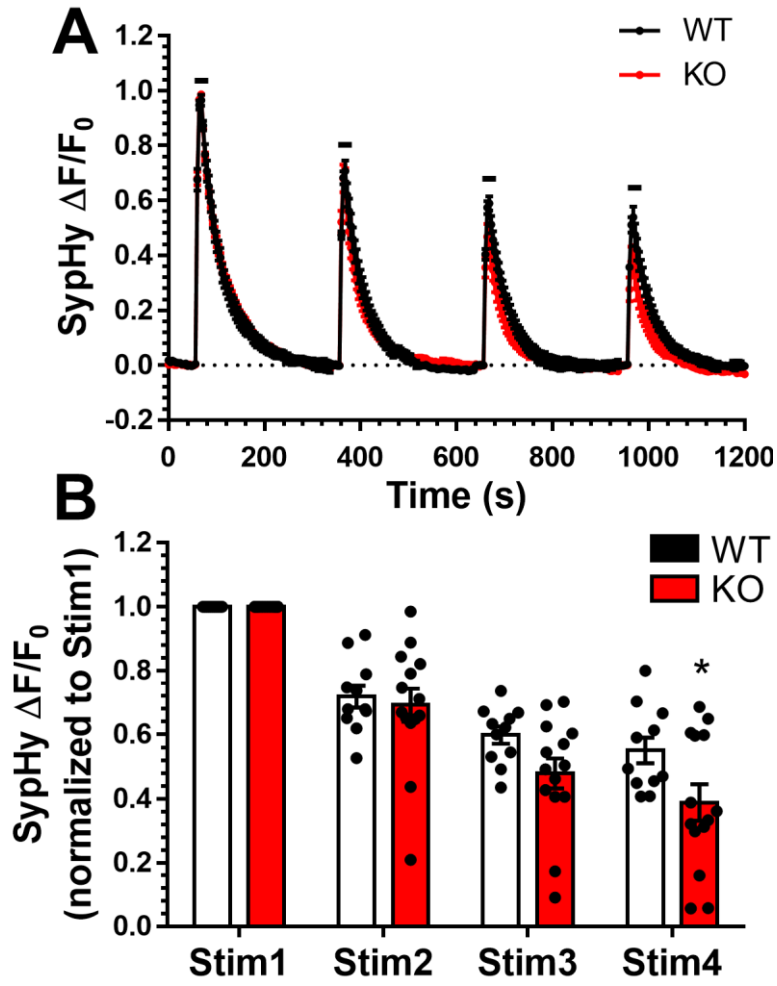

Figure 5. **The ADBE defect in *Fmr1* KO neurons results in decreased presynaptic performance.** Hippocampal neurons derived from either *Fmr1* KO or WT littermate controls were transfected with sypHy on day *in vitro* (*DIV*) 7 and imaged *DIV* 13-15. Transfected neurons were stimulated four times with 40 Hz 10 s at 5 min intervals, before exposure to an alkaline buffer (NH_4Cl). A) Mean traces displaying the average sypHy fluorescent response traces of WT (black) and KO (red) hippocampal neurons is displayed ± SEM. Traces are $\Delta F/F_0$ and normalised to the sypHy peak response to the first train of action potentials. Bar indicates the period of stimulation. B) Mean sypHy peak heights for each 40 Hz 10 s stimulation, normalised to the first ± SEM. 2-way ANOVA * p =0.028, n = 11 for WT and n = 14 for KO.